Research Square

Preprints are preliminary reports that have not undergone peer review.
They should not be considered conclusive, used to inform clinical practice,
or referenced by the media as validated information.

Modeling and Analysis of the Total Accommodation Capability Curve for Active Distribution Networks Considering Demand Response

Haode Yang

19819118027@163.com

State Grid Gansu Electric Power Company Jinchang Power Supply Company

Bin Luo

State Grid Gansu Electric Power Company Jinchang Power Supply Company

Yuxing Wang

State Grid Gansu Electric Power Company Jinchang Power Supply Company

Wenkai Cao

State Grid Gansu Electric Power Company Jinchang Power Supply Company

Wenjun Xu

State Grid Gansu Electric Power Company Jinchang Power Supply Company

Tao Yao

State Grid Gansu Electric Power Company Jinchang Power Supply Company

Xiang Zhang

State Grid Gansu Electric Power Company Jinchang Power Supply Company

Guodong Wang

State Grid Gansu Electric Power Company Jinchang Power Supply Company

Zhiming Yang

State Grid Gansu Electric Power Company Jinchang Power Supply Company

Article

Keywords: total accommodation capability curve, active distribution network, demand response, distributed generation, accommodation capability, flexible load adjustment characteristics

Posted Date: November 26th, 2026

DOI: https://doi.org/10.21203/rs.3.rs-11722311/v1

License: This work is licensed under a Creative Commons Attribution 4.0 International License.
Read Full License

Additional Declarations: No competing interests reported.

Article

Modeling and Analysis of the Total Accommodation Capability Curve for Active Distribution Networks Considering Demand Response

Haode Yang [1,*], Bin Luo [1], Yuxing Wang [1], Wenkai Cao [1], Wenjun Xu [1], Tao Yao [1], Xiang Zhang [1], Guodong Wang [1], and Zhiming Yang [1]

[1] State Grid Gansu Electric Power Company Jinchang Power Supply Company; Jinchang 737100, China;
* Correspondence: 19819118027@163.com

Abstract

To comprehensively characterize the DG accommodation capability of distribution networks with flexible loads participating in demand response (DR), this paper proposes a total accommodation capability (TAC) curve for active distribution networks (ADNs) considering DR. First, a mathematical model of the TAC curve incorporating DR and voltage constraints is established, in which a load adjustment coefficient is introduced to quantify the degree of user participation in DR. Second, a TAC curve calculation algorithm that accounts for flexible load adjustment characteristics is developed to determine the TAC curve indices under different load adjustment coefficients. Third, the impacts of the degree of flexible load participation in DR and the locations of flexible loads on the TAC curve are investigated. The results reveal that the TAC initially increases and then remains constant with increasing load adjustment coefficients only when the flexible loads participating in DR are located downstream of the bottleneck branch. Moreover, the magnitude of TAC improvement may vary depending on the locations of the participating loads. Based on these findings, two measures are proposed to enhance the TAC curve: increasing the load adjustment coefficients of flexible loads downstream of the bottleneck branch and upgrading the capacity of the bottleneck branch. Subsequently, the application of the TAC curve to DR decision-making is demonstrated. Finally, the effectiveness of the proposed method is validated using the IEEE 33-node test system. The proposed TAC curve effectively characterizes the overall DG accommodation capability of active distribution networks considering DR, thereby providing practical guidance for distribution network planning.

Keywords: total accommodation capability curve; active distribution network; demand response; distributed generation; accommodation capability; flexible load adjustment characteristics.

1. Introduction

With the ongoing development of the new-type power system, the penetration of distributed generation (DG), particularly photovoltaic and wind power, in distribution networks has continued to increase, effectively promoting renewable energy utilization and facilitating the transition of the energy structure [1,2]. However, the intermittent, fluctuating, and uncertain nature of DG output [3–5] poses considerable challenges to the secure and economic operation of distribution networks and the effective integration of renewable energy. It also places increasingly stringent demands on the flexibility of power systems [6]. Against this backdrop, accurately quantifying the secure DG hosting limits of distribution networks is of great importance for guiding rational distribution network planning and ensuring secure system operation [7,8].

Existing studies have commonly adopted accommodation capability to characterize the maximum DG output that can be accommodated by distribution networks [9,10], making it an important indicator for quantifying renewable energy accommodation levels and guiding distribution network planning and operation. Extensive research has been conducted on renewable energy accommodation capability in ADNs, covering its conceptual definition [9,10,16], mathematical modeling [11–15,17,18], assessment methods [16,18], and practical applications [16,18]. Regarding accommodation capability assessment, to address the uncertainty associated with renewable energy generation, a Wasserstein

generative adversarial network was employed to characterize the probability distributions of wind and photovoltaic power outputs, and an accommodation capability assessment model integrating deep reinforcement learning was developed to improve assessment efficiency under different operating scenarios [11]. Considering the time-varying operational characteristics of distribution networks, a bi-level PV accommodation capability assessment model was established to jointly evaluate PV deployment and accommodation performance under secure operating constraints [12]. Operational risks and non-anticipativity constraints were incorporated into a multi-stage robust optimization model to quantitatively assess the dynamic boundaries of wind power accommodation capability [13]. From the perspectives of long-term planning and short-term operation, quantitative assessments of wind power accommodation capability in regional power grids were conducted based on system peak-shaving capability and day-ahead unit commitment models, respectively [14]. Furthermore, a maximum PV accommodation capability assessment model for distribution networks was developed by integrating deep learning with distributionally robust joint chance constraints [15]. Regarding accommodation capability enhancement, the coordination of dynamic line regulation and distribution network optimization was investigated to improve line power transfer capability and network operating conditions, thereby increasing DG accommodation capability [16]. Nevertheless, these studies have primarily focused on assessing and enhancing either the maximum accommodation capability or the accommodation capability under specific operating scenarios, and therefore cannot provide a comprehensive characterization of the accommodation capability under different DG output distributions. To comprehensively characterize the DG accommodation capability of ADNs, the concept of the total accommodation capability curve (TAC curve) was proposed based on the security region theory of ADNs, and a corresponding mathematical model was established to characterize the DG output limits along the security boundaries of distribution networks [17]. Furthermore, AC power flow constraints were incorporated into the TAC curve model, and a corresponding calculation method was developed. The proposed method was subsequently applied to distribution line replacement decisions, providing a new analytical basis for distribution network planning [18].

The above review indicates that the TAC curve provides a comprehensive characterization of the DG accommodation capability of distribution networks and is of significant value for distribution network planning [17,18]. However, in practical operation, with the growing importance of flexibility resources, existing TAC curve models have not adequately accounted for demand response (DR) [19] as a flexibility resource. DR guides consumers to proactively adjust their electricity consumption behavior through price-based or incentive-based signals, thereby reshaping load distributions across both temporal and spatial dimensions and effectively enhancing the potential of distribution networks to accommodate renewable energy [20]. Meanwhile, the uncertainty associated with DR [21,22] further increases the complexity of TAC curve calculation. Against this backdrop, accurately assessing the overall DG accommodation capability of ADNs considering DR is essential for guiding distribution network planning and operation. To address this research gap, this paper proposes a mathematical model, a calculation algorithm, and an application method for the TAC curve of ADNs considering DR. The main contributions are summarized as follows:

(1) A mathematical model of the TAC curve considering DR and voltage constraints is proposed.

(2) A TAC curve calculation algorithm that accounts for flexible load adjustment characteristics is developed.

(3) The impacts of DR on the TAC curve are revealed and analyzed, and corresponding measures to enhance DG accommodation capability are proposed.

The remainder of this paper is organized as follows. Section 2 introduces the security region and security boundary of ADNs. Section 3 develops the mathematical model of the TAC curve considering DR and voltage constraints. Section 4 presents a TAC curve calculation algorithm that accounts for flexible load adjustment characteristics. Section 5 validates the effectiveness of the proposed method using the IEEE 33-node test system, investigates the impacts of DR on the TAC curve and corresponding measures for enhancing DG accommodation capability, and demonstrates the application of the TAC curve to DR decision-making. Finally, Section 6 concludes the paper.

2. Preliminary concepts

The TAC curve is constructed by connecting security boundary points located along the outer boundary of the security region. This section first introduces the security region of ADNs and then describes the corresponding security boundaries.

2.1. Security Region Model of ADNs

The distribution system security region (DSSR) of an ADN is defined as the set of all operating points in the state space that satisfy the system security constraints [23]. Depending on the security constraints considered, existing studies have developed an N-0 security region model that satisfies normal operating constraints (i.e., N-0 security) [23,24] and an N-1 security region model that satisfies N-1 security constraints [18]. Since N-0 security is a fundamental requirement for the secure operation of distribution networks and also forms the basis of N-1 security, this paper adopts the N-0 security region (DSSR) model [23,24], as formulated in equation (1).

$$
\begin{aligned}
&\boldsymbol{D}_{\mathrm{DSSR}}=\left\{\boldsymbol{X}_{\mathrm{B}}=\begin{bmatrix}\boldsymbol{X}_{\mathrm{DGB}}\\ \boldsymbol{X}_{\mathrm{LB}}\end{bmatrix}=\begin{bmatrix}\left[S_{\mathrm{DGB},1},\ldots,S_{\mathrm{DGB},x},\ldots,S_{\mathrm{DGB},m}\right]^{\mathrm{T}}\\ \left[S_{\mathrm{LB},1},\ldots,S_{\mathrm{LB},y},\ldots,S_{\mathrm{LB},n}\right]^{\mathrm{T}}\end{bmatrix}\right.\\
&s.t.(1)\begin{cases}-S_{\mathrm{DGB},x}^{\max}\le S_{\mathrm{DGB},x}\le 0,\forall x\in N_{\mathrm{DG}}\\ 0\le S_{\mathrm{LB},y}\le S_{\mathrm{LB},y}^{\max},\forall y\in N_{\mathrm{L}}\end{cases}\\
&s.t.(2)\left\{\boldsymbol{X}_{\mathrm{B}}\left|\begin{array}{l}-c_1\le(1+r)(h'_{11}S_{\mathrm{DGB},1}+\ldots+h'_{1m}S_{\mathrm{DGB},m}\\ \qquad+h'_{1(m+1)}S_{\mathrm{LB},1}+\ldots+h'_{1(m+n)}S_{\mathrm{LB},n})\le c_1\\ -c_2\le(1+r)(h'_{21}S_{\mathrm{DGB},1}+\ldots+h'_{2m}S_{\mathrm{DGB},m}\\ \qquad+h'_{2(m+1)}S_{\mathrm{LB},1}+\ldots+h'_{2(m+n)}S_{\mathrm{LB},n})\le c_2\\ \qquad\ldots\\ -c_k\le(1+r)(h'_{k1}S_{\mathrm{DGB},1}+\ldots+h'_{km}S_{\mathrm{DGB},m}\\ \qquad+h'_{k(m+1)}S_{\mathrm{LB},1}+\ldots+h'_{k(m+n)}S_{\mathrm{LB},n})\le c_k\end{array}\right.\right.
\end{aligned}
\tag{1}
$$

where $\boldsymbol{D}_{\mathrm{DSSR}}$ denotes the N-0 security region of ADN; $\boldsymbol{X}_{\mathrm{B}}$ represents an operating point; $\boldsymbol{X}_{\mathrm{DGB}}$ denotes the DG node power vector component of $\boldsymbol{X}_{\mathrm{B}}$; $S_{\mathrm{DGB},x}$ represents the power injected at the xth DG node; $\boldsymbol{X}_{\mathrm{LB}}$ denotes the load node power vector component of $\boldsymbol{X}_{\mathrm{B}}$; $S_{\mathrm{LB},y}$ represents the power outflow at the yth load node; and m and n denote the numbers of DG nodes and load nodes, respectively.

s.t.(1) denotes the state-space constraints. It considers the capacity limits of DG and load nodes in practical operation, ensuring that their power outputs remain within the secure operating range. Here, $S_{\mathrm{DGB},x}^{\max}$ denotes the upper capacity limit of $S_{\mathrm{DGB},x}$; $S_{\mathrm{LB},y}^{\max}$ denotes the upper capacity limit of $S_{\mathrm{LB},y}$; N_{DG} and N_{L}denote the sets of DG nodes and load nodes, respectively.

s.t.(2) denotes the normal operating constraints. The left-hand-side and right-hand-side constraints represent the reverse and forward power flow security constraints, respectively. They ensure that both reverse and forward power flows do not exceed the capacity limits of network components. Here, r denotes the network loss coefficient, which is determined by performing AC power flow calculations for typical security boundary points; h'_{km} indicates whether the kth constraint involves the mth component, taking a value of 1 if included and 0 otherwise; c_k denotes the capacity of the kth component (branch or upstream electrical equipment).

2.2. Security Boundary Model of ADNs

The outer boundary of the DSSR consists of operating points exhibiting criticality [23], and the set of these points is defined as the security boundary. Reference [25] identifies four distinct types of criticality in ADNs. Among them, the TAC curve investigated in this paper focuses on DG growth criticality, which means that any individual increase in DG output will cause the system to enter an insecure operating state. The mathematical definition of DG growth criticality is as follows: if an operating point $\boldsymbol{X}_{\mathrm{B}}=[S_{\mathrm{DGB},1},\ldots,S_{\mathrm{DGB},x},\ldots,S_{\mathrm{DGB},m},\boldsymbol{X}_{\mathrm{LB}}]$ lies on the upper DG security boundary, i.e., $\boldsymbol{X}_{\mathrm{B}}\in\partial\boldsymbol{D}_{\mathrm{DG}^+}$, and an increase in the output of the xth DG, while all other DG outputs and loads remain unchanged, results in a new operating point $\boldsymbol{X}_{\mathrm{B}}'=[S_{\mathrm{DGB},1},\ldots,S_{\mathrm{DGB},x}+\varepsilon,\ldots,S_{\mathrm{DGB},m},\boldsymbol{X}_{\mathrm{LB}}]$, if $\lim\varepsilon\to 0^+$ and $\forall x\in\{1,2,\ldots,m\}$ hold for $\boldsymbol{X}_{\mathrm{B}}'\notin\partial\boldsymbol{D}_{\mathrm{DG}^+}$, then $\boldsymbol{X}_{\mathrm{B}}$ is said to exhibit DG growth criticality. Operating points exhibiting DG growth criticality are defined as security boundary points, hereafter referred to as boundary points. The set of all boundary points is defined as the upper DG security boundary, hereafter referred to as the DG boundary and denoted by $\partial\boldsymbol{D}_{\mathrm{DG}^+}$. By setting selected reverse power flow constraints in (1) to equality constraints such that all DG variables are covered, an upper

DG security boundary $\beta_{\mathrm{DG}^+,j}$ can be obtained, as formulated in equation (2).

$$\beta_{\mathrm{DG}^+,j}=\left\{X_{\mathrm{B}}\left|\begin{array}{l}-c_1=(1+r)(h'_{11}S_{\mathrm{DGB},1}+\ldots+h'_{1m}S_{\mathrm{DGB},m}+\\ \quad h'_{1(m+1)}S_{\mathrm{LB},1}+\ldots+h'_{1(m+n)}S_{\mathrm{LB},n})\\ \quad\ldots\ldots\\ -c_l=(1+r)(h'_{l1}S_{\mathrm{DGB},1}+\ldots+h'_{lm}S_{\mathrm{DGB},m}+\\ \quad h'_{l(m+1)}S_{\mathrm{LB},1}+\ldots+h'_{l(m+n)}S_{\mathrm{LB},n})\\ -c_{l+1}\le(1+r)(h'_{(l+1)1}S_{\mathrm{DGB},1}+\ldots+h'_{(l+1)m}S_{\mathrm{DGB},m}+\\ \quad h'_{(l+1)(m+1)}S_{\mathrm{LB},1}+\ldots+h'_{(l+1)(m+n)}S_{\mathrm{LB},n})\le c_{l+1}\\ \quad\ldots\ldots\\ -c_k\le(1+r)(h'_{k1}S_{\mathrm{DGB},1}+\ldots+h'_{km}S_{\mathrm{DGB},m}+\\ \quad h'_{k(m+1)}S_{\mathrm{LB},1}+\ldots+h'_{k(m+n)}S_{\mathrm{LB},n})\le c_k\\ h'_{11}+h'_{21}+\ldots+h'_{l1}>0,\\ \quad\ldots\ldots\\ h'_{1m}+h'_{2m}+\ldots+h'_{lm}>0\end{array}\right.\right\} \quad (2)$$

where $\beta_{\mathrm{DG}^+,j}$ denotes the jth DG boundary; l is the number of equality constraints; and k is the total number of constraints. It should be noted that DG growth criticality is ensured by the condition that the sum of the coefficients of DG variables in each equality constraint is greater than zero. The component whose reverse power flow first reaches its capacity limit among the equality constraints defining DG growth criticality, thereby restricting further increases in DG output, is defined as the bottleneck component [24]. Its capacity is an important factor limiting the TAC curve.

3. TAC Curve Model Considering DR

The TAC curve is constructed by arranging all boundary points in the distribution network that satisfy the specified security constraints in ascending order of total DG output [17]. Since the TAC curve is constructed from boundary points, these points are hereafter referred to as TAC curve points. The proposed TAC curve model considering DR is shown in equation (3).

$$\left\{\begin{array}{l}L_{\mathrm{TAC}}=\left\{\left(i,\mathrm{Tot}(\boldsymbol{X}_{\mathrm{DGB},i})\right)\left|\begin{array}{l}\mathrm{Tot}(\boldsymbol{X}_{\mathrm{DGB},i})\le\mathrm{Tot}(\boldsymbol{X}_{\mathrm{DGB},i+1})\\ i\in\{1,2,3\ldots\}\end{array}\right.\right\}\\ s.t.(1)\ \mathrm{Tot}(\boldsymbol{X}_{\mathrm{DGB},i})=\sum_{x=1}^{m}|S_{\mathrm{DGB},x}|\\ s.t.(2)\left\{\begin{array}{l}\boldsymbol{X}_{\mathrm{B},i}=\begin{bmatrix}\boldsymbol{X}_{\mathrm{DGB},i}\\ \boldsymbol{X}_{\mathrm{LB},i}\end{bmatrix}=\begin{bmatrix}\left[S_{\mathrm{DGB},1},\ldots,S_{\mathrm{DGB},x},\ldots,S_{\mathrm{DGB},m}\right]^{\mathrm{T}}\\ \left[S_{\mathrm{LB},1},\ldots,S_{\mathrm{LB},y},\ldots,S_{\mathrm{LB},n}\right]^{\mathrm{T}}\end{bmatrix}\\ -S^{\max}_{\mathrm{DGB},x}\le S_{\mathrm{DGB},x}\le 0,\forall x\in N_{\mathrm{DG}}\\ 0\le S_{\mathrm{LB},y}\le S^{\max}_{\mathrm{L},y},\forall y\in N_{\mathrm{L}}\end{array}\right.\\ s.t.(3)\left\{\begin{array}{l}\boldsymbol{X}_{\mathrm{B},i}\in\boldsymbol{D}_{\mathrm{DG}^+}\\ \boldsymbol{D}_{\mathrm{DG}^+}=\{\beta_{\mathrm{DG}^+,j}\mid j=1,2,3\ldots\}\end{array}\right.\\ s.t.(4)\ \beta_{\mathrm{DG}^+,j}=\\ \left\{\boldsymbol{X}_{\mathrm{B},i}\left|\begin{array}{l}-c_1=(1+r)(h'_{11}S_{\mathrm{DGB},1}+\ldots+h'_{1m}S_{\mathrm{DGB},m}+\ldots\\ \quad+h'_{1(m+s)}\lambda_{\mathrm{LB},s}S_{\mathrm{LB},s}+\ldots+h'_{1(m+n)}S_{\mathrm{LB},n})\\ \quad\ldots\ldots\\ -c_l=(1+r)(h'_{l1}S_{\mathrm{DGB},1}+\ldots+h'_{lm}S_{\mathrm{DGB},m}+\ldots\\ \quad+h'_{l(m+s)}\lambda_{\mathrm{LB},s}S_{\mathrm{LB},s}+\ldots+h'_{l(m+n)}S_{\mathrm{LB},n})\\ -c_{l+1}\le(1+r)(h'_{(l+1)1}S_{\mathrm{DGB},1}+\ldots+h'_{(l+1)m}S_{\mathrm{DGB},m}+\ldots\\ \quad+h'_{(l+1)(m+s)}\lambda_{\mathrm{LB},s}S_{\mathrm{LB},s}+\ldots+h'_{(l+1)(m+n)}S_{\mathrm{LB},n})\le c_{l+1}\\ \quad\ldots\ldots\\ -c_k\le(1+r)(h'_{k1}S_{\mathrm{DGB},1}+\ldots+h'_{km}S_{\mathrm{DGB},m}+\ldots\\ \quad+h'_{k(m+s)}\lambda_{\mathrm{LB},s}S_{\mathrm{LB},s}+\ldots+h'_{k(m+n)}S_{\mathrm{LB},n})\le c_k\\ h'_{11}+h'_{21}+\ldots+h'_{l1}>0,\\ \quad\ldots\ldots\\ h'_{1m}+h'_{2m}+\ldots+h'_{lm}>0\end{array}\right.\right\}\\ s.t.(5)\ \Delta\boldsymbol{U}^{-}_{\mathrm{GB}}\le\Delta\boldsymbol{U}\%=\boldsymbol{K}_{\mathrm{u}}\times\boldsymbol{X}_{\mathrm{B},i}\le\Delta\boldsymbol{U}^{+}_{\mathrm{GB}}\end{array}\right. \quad (3)$$

where L_{TAC} denotes the TAC curve considering DR; Tot($\boldsymbol{X}_{DGB,i}$) represents the accommodation capability of the ith operating point; i is the sequential index of the TAC curve points; and $\boldsymbol{X}_{DGB,i}$ denotes the column vector of DG node power outputs at the ith operating point.

s.t.(1) denotes the constraint that the accommodation capability Tot($\boldsymbol{X}_{DGB,i}$) of an operating point is equal to the sum of the power outputs of all DG nodes at that operating point.

s.t.(2) denotes the state-space constraints. It considers the capacity limits of distribution transformers and DG units in the actual operation of the distribution network, ensuring that load and DG power outputs remain within the prescribed secure operating ranges. Here, $\boldsymbol{X}_{B,i}$ denotes the ith DG boundary point; $\boldsymbol{X}_{DGB,i}$ and $\boldsymbol{X}_{LB,i}$ denote the column vectors of DG node power outputs and load node power outputs at the ith boundary point, respectively.

s.t.(3) denotes the constraint that the operating point $\boldsymbol{X}_{B,i}$ lies on the DG boundary. Here, $\boldsymbol{D}_{DG^+}$ denotes the set of all DG security boundaries.

s.t.(4) denotes the DG growth criticality constraints. It ensures that the equality constraints cover all DG variables, such that every DG variable is constrained by the equality constraints. $\lambda_{LB,s}$ denotes the load adjustment coefficient of user s(s=1,2,…,n), which quantifies the proportion by which the user can increase or decrease electricity consumption in response to dispatch instructions during normal operation. To fully characterize the flexible load adjustment capability on the user side, two types of DR, namely interruptible loads and shiftable loads, are considered simultaneously in *s.t.*(4). Specifically, $0 \le \lambda_{LB,s} \le 1$ represents the proportional load reduction of user s, corresponding to peak-shaving adjustments involving interruptible DR and load shifting out in shiftable DR, and reflects the downward load adjustment capability; $\lambda_{LB,s} = 0$ indicates that user s is allowed to be completely disconnected from the power supply, in which case the downward load adjustment reaches its maximum; $\lambda_{LB,s} = 1$ indicates that user s does not participate in DR; and $\lambda_{LB,s} \ge 1$ represents the proportional load increase of user s, corresponding to valley-filling adjustments involving load shifting in under shiftable DR, thereby reflecting the upward load adjustment flexibility and the contribution of DR to DG accommodation. The load adjustment coefficient quantifies the flexibility of DR participants and its contribution to DG accommodation.. This approach has been widely adopted in existing studies [26].

s.t.(5) denotes the node voltage constraints. It ensures that the voltage deviations at DG boundary points do not exceed the permissible limits. Here, $\Delta \boldsymbol{U}$ denotes the node voltage deviation vector, $\boldsymbol{K}_u$ denotes the coefficient matrix, and $\Delta \boldsymbol{U}_{GB}^-$ and $\Delta \boldsymbol{U}_{GB}^+$ denote the lower and upper voltage deviation limits specified by the applicable national standard, respectively, which are set to −7% and 7%, respectively, for 10kV distribution networks [27].

Compared with the existing model [17], the proposed TAC curve model incorporates DR to enable flexible load adjustment and additionally accounts for voltage constraints, thereby providing a more realistic characterization of the overall DG accommodation capability of distribution networks under actual operating conditions.

4. TAC Curve Calculation Algorithm Considering Flexible Load Adjustment Characteristics

To quantify the overall DG accommodation capability of distribution networks under DR, a TAC curve calculation algorithm that accounts for flexible load adjustment characteristics is proposed. The algorithm considers the load adjustment capability provided by flexible loads participating in DR and is applicable to ADN within a specific power supply area. The calculation procedure is illustrated in Figure 1, and the specific steps are as follows:

Step 1: Construct a multidimensional operating-variable state space consisting of loads [0, $S_{LB,y}^{max}$] and DG outputs [$-S_{DGB,x}^{max}$,0] according to equation (3) *s.t.*(2). Discretize the state space with a sampling step size of d to generate H sampling points that approximately cover the entire state space.

$$H = \prod_{x=1}^{m}\left(1 + \frac{\left|S_{DGB,x}^{max}\right|}{d}\right)\prod_{y=1}^{n}\left(1 + \frac{S_{LB,y}^{max}}{d}\right) \quad (4)$$

Step 2: Set the load adjustment coefficient $\lambda_{LB,s}$ according to the DR participation level and the locations of flexible loads. First, the discretized sampling points generated in Step 1 that satisfy the DG growth criticality constraints in equation (3) *s.t.*(4) are selected to obtain the initial TAC curve points accounting for flexible load adjustment characteristics. Subsequently, the OpenDSS power flow solver is used to calculate the voltage deviations at each node for all sampling points. The results are then checked against the node voltage constraints in equation (3) *s.t.*(5), and sampling points with voltage violations are discarded. Finally, the valid TAC curve points satisfying the voltage constraints under the $\lambda_{LB,s}$ scenario are obtained.

Step 3: Calculate the accommodation capability Tot($\boldsymbol{X}_{DGB,i}$) corresponding to each valid TAC curve point under the

$\lambda_{LB,s}$ scenario according to equation (3) *s.t.*(1), and arrange the points in ascending order of accommodation capability. Taking the sequential index i of the sorted points as the abscissa and the corresponding accommodation capability Tot($\boldsymbol{X}_{DGB,i}$) as the ordinate, the TAC curve under the $\lambda_{LB,s}$ scenario is obtained.

Step 4: Calculate the maximum, minimum, and average TAC values based on the TAC curve obtained in Step 3. The maximum TAC (TAC) represents the highest DG accommodation capability among all curve points, whereas the minimum TAC (TAC_{min}) represents the lowest. The average TAC ($\overline{TAC}$) is used to characterize the overall accommodation capability represented by the curve.

By comparing the aforementioned indices under different $\lambda_{LB,s}$ scenarios, the impacts of flexible load adjustment characteristics on the DG accommodation capability of distribution networks are quantitatively analyzed, thereby evaluating the changes in DG accommodation capability resulting from the participation of interruptible and shiftable loads in DR.

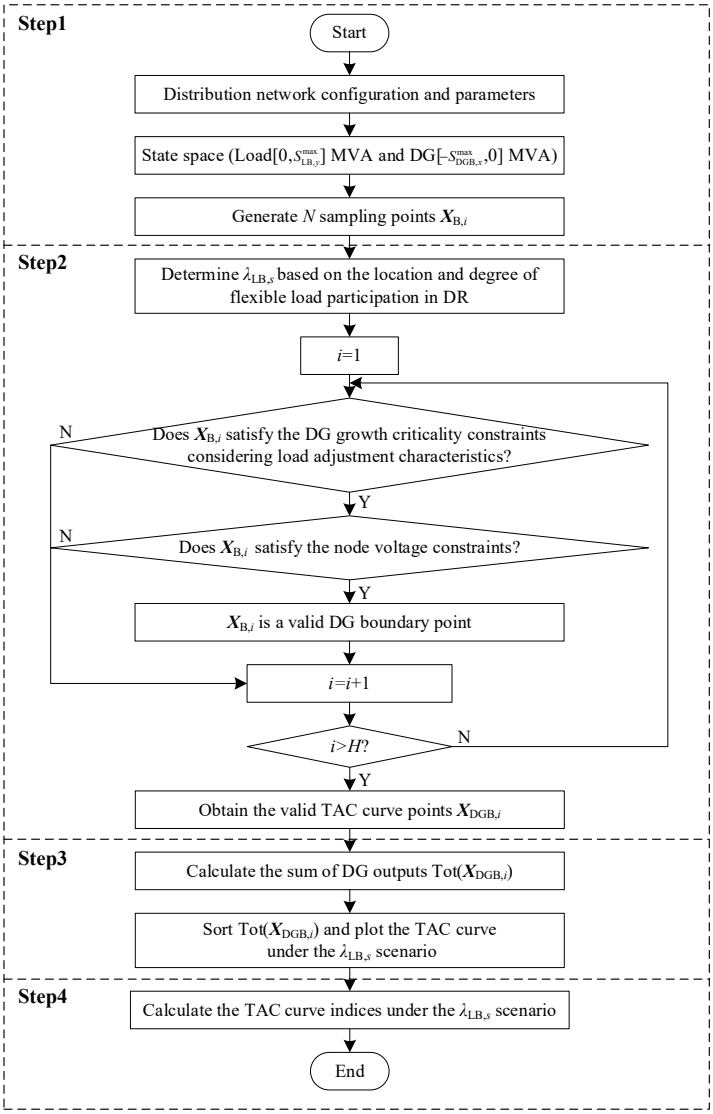

Figure 1. Flowchart of the TAC curve calculation algorithm considering flexible load adjustment characteristics.

Compared with the existing algorithm [17], the proposed TAC curve calculation algorithm accounts for the adjustment characteristics of flexible loads participating in DR during the actual operation of distribution networks. It enables the calculation of TAC curve indices under different DR scenarios and quantifies the system's DG accommodation capability in terms of specific numerical ranges based on these indices, thereby providing a basis for planners to accurately assess the overall DG accommodation capability of distribution networks.

5. Case Study

5.1. Description of the IEEE 33-Node Test System

The proposed method is demonstrated in detail using the IEEE 33-node test system shown in Figure 2. Each branch has a length of 1.00 km, and the longest path extends from node 0 to node 17, with a total length of 17.00 km. DG units are connected to nodes 4, 6, and 27. Loads located between adjacent DG nodes are aggregated [17] into four virtual load nodes, denoted by L_1, L_2, L_3, and L_4. The resulting network configuration after load aggregation is shown in Figure 3. The parameters of the test system are listed in Table 1.

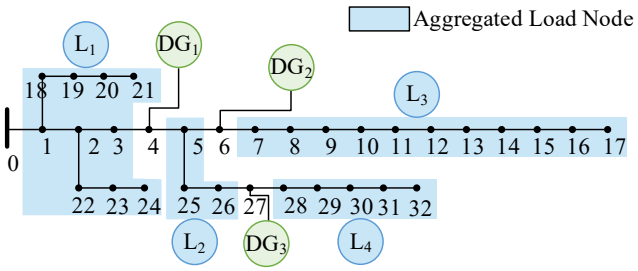

Figure 2. IEEE 33-node active distribution network.

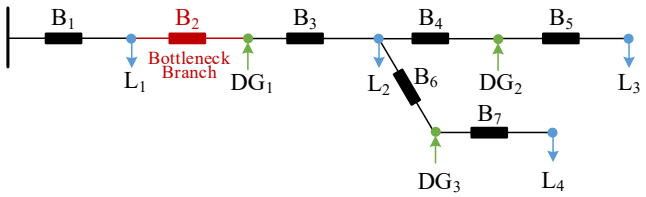

Figure 3. Simplified structure of the IEEE 33-node test system.

Table 1. Parameters of the IEEE 33-node test system.

Parameter	Value
Feeder Type	YJV22-3×240
Unit Impedance/(Ω/km)	0.20+j0.19
The network loss coefficient *r*	2%
Feeder capacity/MVA	1.60
Load power factor	0.95
DG power factor	0.95
Load power range/MVA	[0.00,1.00]
DG output range/MVA	[-1.80,0.00]

5.2. Analysis of the Impacts of DR on the TAC Curve

The impacts of DR on the TAC curve are analyzed in terms of both the degree of flexible load participation in DR and load location. The proposed method is demonstrated in detail using the test system shown in Figure 3.

5.2.1 Impact of DR Participation Level on the TAC Curve

（1）DR Load Adjustment Coefficient Increasing Scenario

To investigate the impact of the degree of flexible load participation in DR on the TAC curve, the TAC curves for load $S_{LB,4}$ in the IEEE 33-node test system are calculated using the algorithm presented in Section 4. The calculation procedure and results are presented as follows. The load adjustment coefficient $\lambda_{LB,4}$ of the user participating in DR ranges from 1.00 to 2.00.

Step 1: Uniformly sample the state space (load: [0.00, 1.00] MVA; DG: [−1.80, 0.00] MVA) at an interval of 0.10, generating a total of $\prod_{x=1}^{3}(1+\frac{|-1.8|}{0.1})\prod_{y=1}^{4}(1+\frac{1.0}{0.1})$ =100,422,619 sampling points.

Step 2: Taking the load adjustment coefficient $\lambda_{LB,4}$ as an example, the TAC curve model for the IEEE 33-node test system is obtained, as formulated in equation (5).

$$
\begin{cases}
L_{\mathrm{TAC}}=\left\{\left(i,\mathrm{Tot}(\boldsymbol{X}_{\mathrm{DGB},i})\right)\middle|\begin{matrix}\mathrm{Tot}(\boldsymbol{X}_{\mathrm{DGB},i})\le\mathrm{Tot}(\boldsymbol{X}_{\mathrm{DGB},i+1})\\ i\in\{1,2,3...\}\end{matrix}\right\}\\
s.t.(1)\ \mathrm{Tot}(\boldsymbol{X}_{\mathrm{DGB},i})=\sum_{x=1}^{3}|S_{\mathrm{DGB},x}|\\
s.t.(2)\begin{cases}\boldsymbol{X}_{\mathrm{B},i}=\begin{bmatrix}\boldsymbol{X}_{\mathrm{DGB},i}\\ \boldsymbol{X}_{\mathrm{LB},i}\end{bmatrix}=\begin{bmatrix}\left[S_{\mathrm{DGB},1},S_{\mathrm{DGB},2},S_{\mathrm{DGB},3}\right]^{\mathrm{T}}\\ \left[S_{\mathrm{LB},1},S_{\mathrm{LB},2},S_{\mathrm{LB},3},S_{\mathrm{LB},4}\right]^{\mathrm{T}}\end{bmatrix}\\ -1.80\le S_{\mathrm{DGB},x}\le 0\ \mathrm{MVA},\forall x\in N_{\mathrm{DG}}\\ 0\le S_{\mathrm{LB},y}\le 1.00\ \mathrm{MVA},\forall y\in N_{\mathrm{L}}\end{cases}\\
s.t.(3)\begin{cases}\boldsymbol{X}_{\mathrm{B},i}\in\boldsymbol{D}_{\mathrm{DG}^+}\\ \boldsymbol{D}_{\mathrm{DG}^+}=\{\beta_{\mathrm{DG}^+,1}\}\end{cases}\\
s.t.(4)\ \beta_{\mathrm{DG}^+,1}=\\
\left\{\boldsymbol{X}_{\mathrm{B},i}\middle|\begin{matrix}S_{\mathrm{LB},2}+S_{\mathrm{LB},3}+\lambda_{\mathrm{LB},4}S_{\mathrm{LB},4}+S_{\mathrm{DGB},1}+S_{\mathrm{DGB},2}+S_{\mathrm{DGB},3}=-1.60\\ |\,S_{\mathrm{LB},1}+S_{\mathrm{LB},2}+S_{\mathrm{LB},3}+\lambda_{\mathrm{LB},4}S_{\mathrm{LB},4}+S_{\mathrm{DGB},1}+S_{\mathrm{DGB},2}+S_{\mathrm{DGB},3}\,|\le 1.60\\ |\,S_{\mathrm{LB},2}+S_{\mathrm{LB},3}+\lambda_{\mathrm{LB},4}S_{\mathrm{LB},4}+S_{\mathrm{DGB},2}+S_{\mathrm{DGB},3}\,|\le 1.60\\ |\,S_{\mathrm{LB},3}+S_{\mathrm{DGB},2}\,|\le 1.60\\ |\,S_{\mathrm{LB},3}\,|\le 1.60\\ |\,\lambda_{\mathrm{LB},4}S_{\mathrm{LB},4}+S_{\mathrm{DGB},3}\,|\le 1.60\\ |\,\lambda_{\mathrm{LB},4}S_{\mathrm{LB},4}\,|\le 1.60\end{matrix}\right\}\\
s.t.(5)\ -7\%\le\Delta\boldsymbol{U}\%=\boldsymbol{K}_{\mathrm{u}}\times\boldsymbol{X}_{\mathrm{B},i}\le 7\%
\end{cases}
\tag{5}
$$

In equation (5), the DG growth criticality equality constraint $S_{\mathrm{LB},2}+S_{\mathrm{LB},3}+\lambda_{\mathrm{LB},4}S_{\mathrm{LB},4}+S_{\mathrm{DGB},1}+S_{\mathrm{DGB},2}+S_{\mathrm{DGB},3}=-1.60$ MVA covers all DG variables, ensuring that the DG boundary points satisfy the criticality condition. Meanwhile, the value of 1.60 MVA on the right-hand side of the equality constraint corresponds to the capacity of branch B_2, indicating that the reverse power flow in branch B_2 reaches its capacity limit first, thereby restricting any further increase in DG output. Therefore, branch B2 is identified as the bottleneck branch, as highlighted in red in Figure 3.

A total of 6,038 boundary points satisfying the DG growth criticality constraints in *s.t.*(4) are selected from the sampling points generated in Step 1. Subsequently, the OpenDSS power flow solver is used to calculate the nodal voltage deviations at all boundary points. The calculated voltages are then checked against the constraints in *s.t.*(5). Finally, 6,036 valid TAC curve points are retained. The detailed data of the TAC curve points, together with their maximum voltage deviations $\Delta U_{\max}$ and the corresponding nodes $N_{\max}$, under the $\lambda_{\mathrm{LB},4}$=2.00 scenario are presented in Table 2.

Step 3: Plot the TAC curve under the $\lambda_{\mathrm{LB},4}$=2.00 scenario based on the data in Table 2, with the results shown in Figure 4. It should be noted that the TAC curve in Figure 4 contains 37 horizontal segments. This is because multiple TAC curve points may correspond to the same accommodation capability value, indicating that different load or DG distribution patterns may yield identical accommodation capability. For example, a TAC value of 2.60 MVA corresponds to 260 TAC curve points.

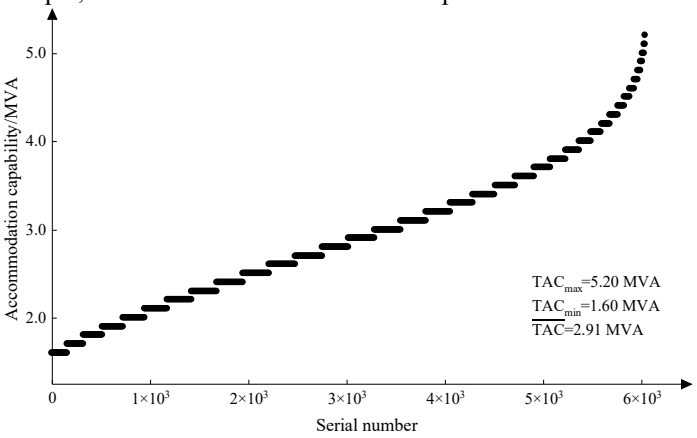

Figure 4. TAC curve for $\lambda_{\mathrm{LB},4}$=2.00.

Step 4: As shown in Figure 4, when the load adjustment coefficient $\lambda_{\mathrm{LB},4}$=2.00, the minimum DG accommodation capability ($\mathrm{TAC}_{\min}$), maximum DG accommodation capability (TAC), and average DG accommodation capability ($\overline{\mathrm{TAC}}$)of the distribution network are 1.60 MVA, 5.20 MVA, and 2.91 MVA, respectively. These results indicate that the

overall DG accommodation capability range of the distribution network under this scenario is [1.60, 5.20] MVA.

Table 2. TAC curve points of the IEEE 33-node test system under the scenario of $\lambda_{LB,4}$=2.00.

i	$X_{B,i}$=[$S_{LB,1}$, $S_{LB,2}$, $S_{LB,3}$, $S_{LB,4}$, $S_{DGB,1}$, $S_{DGB,2}$, $S_{DGB,3}$] MVA	Tot($X_{DGB,i}$)/MVA	ΔU_{max}/%	N_{max}
1	[0, 0, 0, 0, -0.1, -0.1, -1.4]	1.60	1.60%	$S_{LB,4}$
2	[0, 0, 0, 0, -0.1, -0.6, -0.9]	1.60	1.47%	$S_{LB,4}$
	…			
3032	[0, 0, 0.1, 0.6, -1.2, -1.4, -0.3]	2.90	2.96%	$S_{LB,3}$
	…			
6035	[0, 1, 1, 0.8, -1.8, -1.7, -1.7]	5.20	6.95%	$S_{LB,3}$
6036	[0, 1, 1, 0.8, -1.8, -1.8, -1.6]	5.20	6.97%	$S_{LB,3}$

Furthermore, the TAC curve indices are calculated for load adjustment coefficients $\lambda_{LB,4}$ gradually increasing from 1.00 to 2.00. The results are presented in Table 3, and the TAC data in Table 3 are visualized in Figure 5.

Table 3. TAC curve indices of the IEEE 33-node test system under the scenario of increasing $\lambda_{LB,4}$.

$\lambda_{LB,4}$	TAC/MVA	TAC_{min}/MVA	$\overline{TAC}$ /MVA	Range/MVA
1.00	4.60	1.60	2.87	[1.60,4.60]
1.10	4.70	1.60	2.88	[1.60,4.70]
1.20	4.80	1.60	2.89	[1.60,4.80]
1.30	4.90	1.60	2.89	[1.60,4.90]
1.40	5.00	1.60	2.90	[1.60,5.00]
1.50	5.10	1.60	2.91	[1.60,5.10]
1.60-2.00	5.20	1.60	2.91	[1.60,5.20]

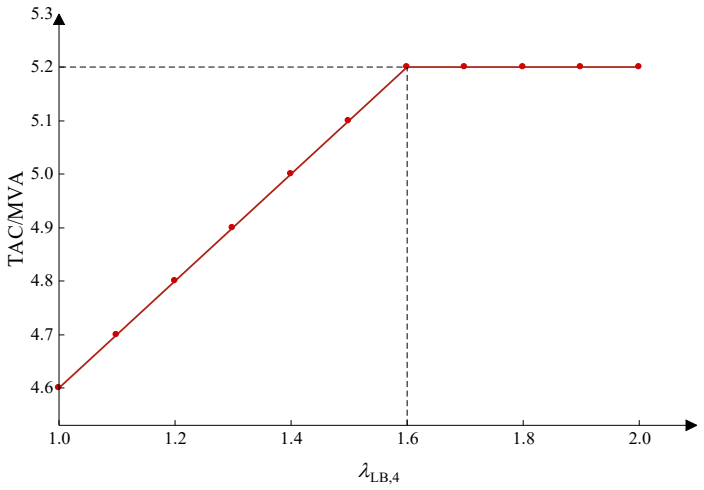

Figure 5. TAC of the IEEE 33-node test system under the scenario of increasing $\lambda_{LB,4}$.

The results in Table 3 and Figure 5 lead to the following conclusions: as the load adjustment coefficient $\lambda_{LB,4}$ increases, the TAC initially increases and then remains constant, whereas TAC_{min} remains unchanged.

A general theoretical analysis of the aforementioned relationship based on the proposed model is presented as follows:

1）As the load adjustment coefficient $\lambda_{LB,s}$ increases, the load power $\lambda_{LB,s}S_{LB,s}$ of the user participating in DR increases, resulting in a reduction in the reverse power flow through the bottleneck branch. According to the DG growth criticality equality constraint $(1+r)(\sum_{x=1}^{m} h'_{1x} S_{DGB,x} + \sum_{y=m+1}^{m+s-1} h'_{1y} S_{LB,y} + h'_{1(m+s)} \lambda_{LB,s} S_{LB,s} + \sum_{y=m+s+1}^{m+n} h'_{1y} S_{LB,y}) = -c_1$, to maintain the bottleneck branch at its rated capacity $|\sum_{x=1}^{m} S_{DGB,x}|$ must increase. Consequently, TAC=$|\sum_{x=1}^{m} S_{DGB,x}|$ increases.

2） As $\lambda_{LB,s}$ continues to increase, $|\sum_{x=1}^{m} S_{DGB,x}|$ reaches a constant value due to the capacity constraint. Consequently, TAC=$|\sum_{x=1}^{m} S_{DGB,x}|$ remains unchanged.

Case Study on the Impact of DR Participation Level on the TAC Curve:

1） Analysis of the impact of DR participation level on the TAC curve: As $\lambda_{LB,4}$ gradually increases from 1.00 to 1.60, the conditions $S_{LB,2}$=$S_{LB,3}$=$S_{LB,4}$=1.00 MVA and $S_{DGB,1}$=$S_{DGB,2}$=$S_{DGB,3}$=-1.80 MVA are satisfied. According to the DG growth criticality equality constraint $S_{LB,2}$+$S_{LB,3}$+$\lambda_{LB,4}S_{LB,4}$+$S_{DGB,1}$+$S_{DGB,2}$+$S_{DGB,3}$=-1.60 MVA, it follows that $|\sum_{x=1}^{3} S_{DGB,x}|$=|-1.60-($S_{LB,2}$+$S_{LB,3}$+$\lambda_{LB,4}S_{LB,4}$)|=|-3.60-$\lambda_{LB,4}$|. As $\lambda_{LB,4}$ gradually increases from 1.00 to 1.60, TAC=$|\sum_{x=1}^{3} S_{DGB,x}|$ increases from 4.60 to 5.20 MVA, reaching a maximum value of 5.20 MVA. When $\lambda_{LB,4}$ continues to increase, the constraint $|\lambda_{LB,4}S_{LB,4}|$≤1.60 MVA indicates that $\lambda_{LB,4}S_{LB,4}$ reaches its upper capacity limit of 1.60 MVA and can no longer increase. Consequently, TAC=$|\sum_{x=1}^{3} S_{DGB,x}|$≤5.20 MVA. Therefore, the TAC reaches 5.20 MVA and remains constant thereafter.

2） Analysis of the impact of DR participation level on TAC_{min}: When TAC_{min} is reached, the conditions $S_{LB,2}$=$S_{LB,3}$=$S_{LB,4}$=0.00 MVA are satisfied. According to the equality constraint $S_{LB,2}$+$S_{LB,3}$+$\lambda_{LB,4}S_{LB,4}$+$S_{DGB,1}$+$S_{DGB,2}$+$S_{DGB,3}$=-1.60 MVA, it follows that TAC_{min}=$|\sum_{x=1}^{3} S_{DGB,x}|$=1.60 MVA, which remains constant regardless of the load adjustment coefficient $\lambda_{LB,4}$.

（2）DR Load Adjustment Coefficient Decreasing Scenario

The TAC curve indices for the scenario in which the load adjustment coefficient $\lambda_{LB,4}$ decreases from 1.00 to 0.00 are presented in Table 4. The corresponding TAC data are illustrated in Figure 6.

Table 4. TAC curve indices of the IEEE 33-node test system under the scenario of decreasing $\lambda_{LB,4}$.

$\lambda_{LB,4}$	TAC/MVA	TAC_{min}/MVA	$\overline{TAC}$ /MVA	Range/MVA
1.00	4.60	1.60	2.87	[1.60,4.60]
0.90	4.50	1.60	2.86	[1.60,4.50]
0.80	4.40	1.60	2.84	[1.60,4.40]
0.70	4.30	1.60	2.83	[1.60,4.30]
0.60	4.20	1.60	2.81	[1.60,4.20]
0.50	4.10	1.60	2.78	[1.60,4.10]
0.40	4.00	1.60	2.76	[1.60,4.00]
0.30	3.90	1.60	2.73	[1.60,3.90]
0.20	3.80	1.60	2.70	[1.60,3.80]
0.10	3.70	1.60	2.65	[1.60,3.70]
0.00	3.60	1.60	2.60	[1.60,3.60]

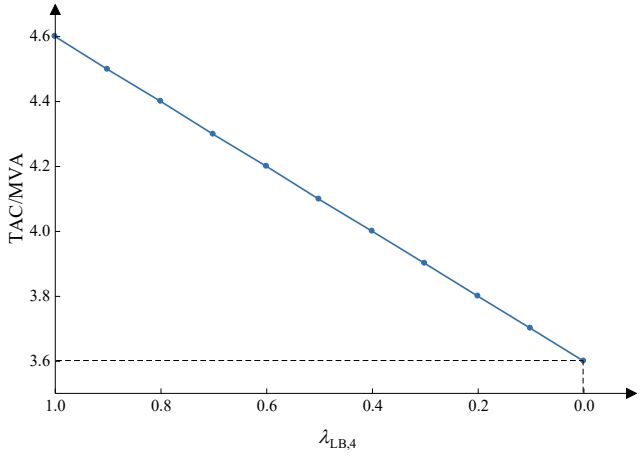

Figure 6. TAC of the IEEE 33-node test system under the scenario of decreasing $\lambda_{LB,4}$.

The results in Table 4 and Figure 6 lead to the following conclusions: as the load adjustment coefficient $\lambda_{LB,4}$ decreases, the TAC decreases, whereas TAC_{min} remains unchanged.

A general theoretical analysis of the aforementioned relationship based on the proposed model is presented as follows:

As the load adjustment coefficient $\lambda_{LB,s}$ decreases, the load power $\lambda_{LB,s}S_{LB,s}$ of the user participating in DR decreases, resulting in an increase in the reverse power flow through the bottleneck branch. To maintain the bottleneck branch at its rated capacity, according to the DG growth criticality equality constraint $(1+r)(\sum_{x=1}^{m} h'_{1x} S_{DGB,x} + \sum_{y=m+1}^{m+s-1} h'_{1y} S_{LB,y} + h'_{1(m+s)} \lambda_{LB,s} S_{LB,s} + h'_{1(m+s)} \lambda_{LB,s} S_{LB,s} + \sum_{y=m+s+1}^{m+n} h'_{1y} S_{LB,y}) = -c_1$, $|\sum_{x=1}^{m} S_{DGB,x}|$ must decrease. Consequently, TAC= $|\sum_{x=1}^{m} S_{DGB,x}|$ decreases.

Case study on the impact of DR participation level on the TAC curve:

1）Analysis of the impact of DR participation level on TAC: As the load adjustment coefficient $\lambda_{LB,4}$ gradually decreases from 1.00 to 0.00, the conditions $S_{LB,2}=S_{LB,3}=S_{LB,4}=1.00$ MVA are satisfied. According to the DG growth criticality equality constraint $S_{LB,2}+S_{LB,3}+\lambda_{LB,4}S_{LB,4}+S_{DGB,1}+S_{DGB,2}+S_{DGB,3}=-1.60$ MVA, it follows that $|\sum_{x=1}^{3} S_{DGB,x}| = |-1.60-(S_{LB,2}+S_{LB,3}+\lambda_{LB,4}S_{LB,4})| = |-3.60-\lambda_{LB,4}|$. As $\lambda_{LB,4}$ decreases from 1.00 to 0.00, $TAC=|\sum_{x=1}^{3} S_{DGB,x}|$ gradually decreases from 4.60 to 3.60 MVA, reaching a minimum value of 3.60 MVA.

2）Analysis of the impact of DR participation level on TAC_{min}: When TAC_{min} is reached, $S_{LB,2}=S_{LB,3}=S_{LB,4}=0.00$ MVA. According to the equality constraint $S_{LB,2}+S_{LB,3}+\lambda_{LB,4}S_{LB,4}+S_{DGB,1}+S_{DGB,2}+S_{DGB,3}=-1.60$ MVA, it follows that $TAC_{min}=|\sum_{x=1}^{3} S_{DGB,x}|$ =1.60 MVA, which remains constant and is independent of the load adjustment coefficient $\lambda_{LB,4}$.

5.2.2 Impact of DR Location on the TAC Curve

To investigate the impact of DR location on the TAC curve, four scenarios are established using the IEEE 33-node test system described in Section 5.1. DR is implemented at load nodes $S_{LB,1}$, $S_{LB,3}$, $S_{LB,4}$, and $S_{LB,2}$, respectively. Among these load nodes, $S_{LB,1}$ is located upstream of the bottleneck branch B_2 in Figure 2, whereas $S_{LB,3}$, $S_{LB,4}$, and $S_{LB,2}$ are located downstream of the bottleneck branch B_2.

Table 5. TAC curve indices of the IEEE 33-node test system considering DR at different locations.

$\lambda_{LB,s}$	TAC/MVA			$\overline{TAC}$ /MVA			TAC_{min}/MVA
	Upstream of bottleneck branch B_2	Downstream of bottleneck branch B_2		Upstream of bottleneck branch B_2	Downstream of bottleneck branch B_2		
	Node $S_{LB,1}$	Node $S_{LB,3}$/$S_{LB,4}$	Node $S_{LB,2}$	Load Node $S_{LB,1}$	Node $S_{LB,3}$/$S_{LB,4}$	Node $S_{LB,2}$	Node $S_{LB,1}$/ $S_{LB,3}$/$S_{LB,4}$/$S_{LB,2}$
0.00	4.6	3.60	3.60	2.87	2.60	2.60	1.60
0.10		3.70	3.70		2.65	2.65	
0.20		3.80	3.80		2.70	2.70	
0.30		3.90	3.90		2.73	2.73	
0.40		4.00	4.00		2.76	2.76	
0.50		4.10	4.10		2.78	2.78	
0.60		4.20	4.20		2.81	2.81	
0.70		4.30	4.30		2.83	2.83	
0.80		4.40	4.40		2.84	2.84	
0.90		4.50	4.50		2.86	2.86	
1.00		4.60	4.60		2.87	2.87	
1.10		4.70	4.70		2.88	2.88	
1.20		4.80	4.80		2.89	2.89	
1.30		4.90	4.90		2.89	2.89	

1.40	5.00	5.00	2.90	2.90
1.50	5.10	5.10	2.91	2.91
1.60	5.20	5.20	2.91	2.91
1.70	5.20	5.30	2.91	2.91
1.80-2.00	5.20	5.40	2.91	2.91

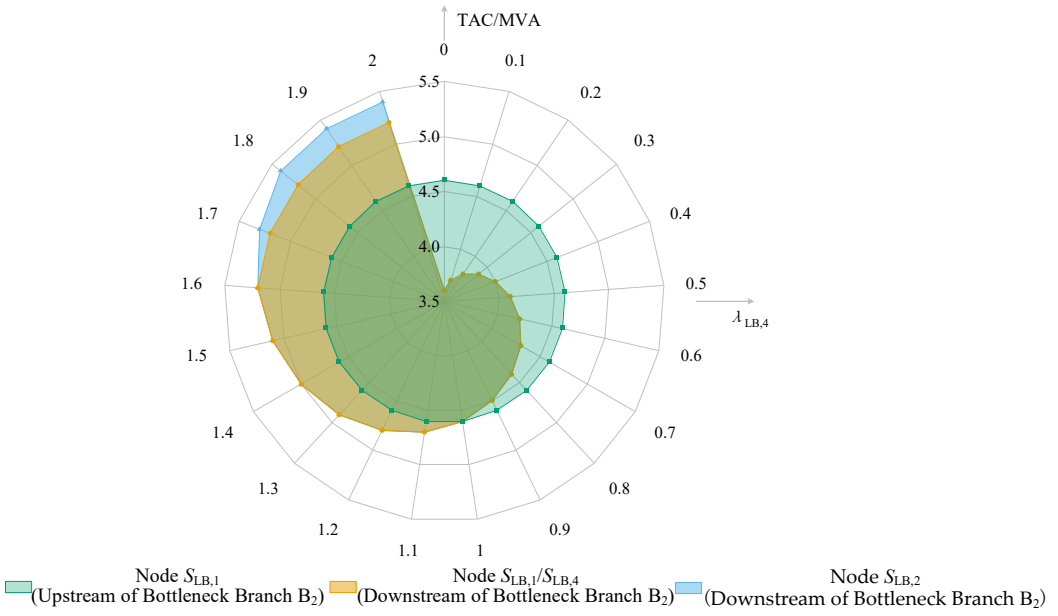

Figure 7. TAC of the IEEE 33-node test system with increasing $\lambda_{LB,s}$ at different load locations.

The results in Table 5 and Figure 7 lead to the following conclusions:

Conclusion 1: When the load participating in DR is located upstream of the bottleneck branch, the TAC curve remains unchanged as the load adjustment coefficient increases.

Conclusion 2: When the load participating in DR is located downstream of the bottleneck branch, the TAC initially increases and then remains constant as the load adjustment coefficient increases. Moreover, the magnitude of the TAC increase may vary depending on the location of the load participating in DR.

A general theoretical analysis of the aforementioned relationship based on the proposed model is presented as follows:

1）When the load participating in DR is located upstream of the bottleneck branch, an increase in the load adjustment coefficient $\lambda_{LB,s}$ leads to an increase in the load power $\lambda_{LB,s}S_{LB,s}$ participating in DR. According to the DG growth criticality equality constraint $(1+r)(\sum_{x=1}^{m} h'_{1x} S_{DGB,x} + \sum_{y=m+1}^{m+s-1} h'_{1y} S_{LB,y} + h'_{1(m+s)} \lambda_{LB,s} S_{LB,s} + \sum_{y=m+s+1}^{m+n} h'_{1y} S_{LB,y}) = -c_1$, all loads $S_{LB,s}$ participating in DR are located downstream of the bottleneck branch. Therefore, DR participation by loads upstream of the bottleneck branch does not affect the DG growth criticality equality constraint, and consequently does not affect $|\sum_{x=1}^{m} S_{DGB,x}|$. Thus, TAC=$|\sum_{x=1}^{m} S_{DGB,x}|$ remains unchanged.

2）When the load participating in DR is located downstream of the bottleneck branch, according to the DG growth criticality equality constraint $(1+r)(\sum_{x=1}^{m} h'_{1x} S_{DGB,x} + \sum_{y=m+1}^{m+s-1} h'_{1y} S_{LB,y} + h'_{1(m+s)} \lambda_{LB,s} S_{LB,s} + \sum_{y=m+s+1}^{m+n} h'_{1y} S_{LB,y}) = -c_1$, an increase in the load adjustment coefficient $\lambda_{LB,s}$ leads to an increase in the load power $\lambda_{LB,s}S_{LB,s}$ participating in DR. Consequently, the reverse power flow through the bottleneck branch decreases. To maintain the bottleneck branch at its rated capacity, $|\sum_{x=1}^{m} S_{DGB,x}|$ must increase. Therefore, TAC=$|\sum_{x=1}^{m} S_{DGB,x}|$ increases.

Case study on the impact of DR location on the TAC curve:

1）When the load participating in DR is located upstream of the bottleneck branch, as $\lambda_{LB,1}$ increases from 0.00 to

2.00, the load power $\lambda_{LB,1}S_{LB,1}$ participating in DR increases. According to the DG growth criticality equality constraint $S_{LB,2}+S_{LB,3}+S_{LB,4}+S_{DGB,1}+S_{DGB,2}+S_{DGB,3}$=-1.60 MVA, the upstream load $S_{LB,1}$ of bottleneck branch B_2 is not included in the equality constraint. Therefore, an increase in $\lambda_{LB,1}S_{LB,1}$ does not affect the equality constraint. It follows that $|\sum_{x=1}^{3} S_{DGB,x}|$ =|-1.60-($S_{LB,2}+S_{LB,3}+S_{LB,4}$)|=4.60 MVA remains unchanged. Consequently, TAC=$|\sum_{x=1}^{3} S_{DGB,x}|$=4.60 MVA remains constant.

2）When the load participating in DR is located downstream of the bottleneck branch, as $\lambda_{LB,4}$ increases from 0.00 to 1.60, the load power $\lambda_{LB,4}S_{LB,4}$ participating in DR increases. According to the DG growth criticality equality constraint $S_{LB,2}+S_{LB,3}+\lambda_{LB,4}S_{LB,4}+S_{DGB,1}+S_{DGB,2}+S_{DGB,3}$=-1.60 MVA, it follows that $|\sum_{x=1}^{3} S_{DGB,x}|$=|-1.60-($S_{LB,2}+S_{LB,3}+\lambda_{LB,4}S_{LB,4}$)|=|-3.60-$\lambda_{LB,4}$|. Consequently, the TAC=$|\sum_{x=1}^{3} S_{DGB,x}|$ increases gradually from 3.60 to 5.20 MVA as $\lambda_{LB,4}$ increases from 0.00 to 1.60, reaching a maximum value of 5.20 MVA. The same analysis applies when load $S_{LB,3}$ participates in DR.

Further analysis reveals that the extent of TAC improvement may vary depending on the location of the load participating in DR at different positions downstream of bottleneck branch B2. This is verified as follows:

1）As the load adjustment coefficient $\lambda_{LB,4}$ increases from 1.60 to 2.00, the conditions $S_{LB,2}=S_{LB,3}=S_{LB,4}$=1.00 MVA and $S_{DGB,1}=S_{DGB,2}=S_{DGB,3}$=-1.80 MVA are satisfied. Since $|\lambda_{LB,4}S_{LB,4}|\leq$1.60, the load power $\lambda_{LB,4}S_{LB,4}$ participating in DR remains constant after reaching its capacity limit of 1.60 MVA. Consequently, TAC=$|\sum_{x=1}^{3} S_{DGB,x}|$=|-1.60-($S_{LB,2}+S_{LB,3}+\lambda_{LB,4}S_{LB,4}$)|=|-3.60-$\lambda_{LB,4}$| reaches 5.20 MVA and remains constant thereafter. The same analysis applies when load $S_{LB,3}$ participates in DR.

2）As the load adjustment coefficient $\lambda_{LB,2}$ increases from 0.00 to 2.00, the conditions $S_{LB,2}=S_{LB,3}=S_{LB,4}$=1.00 MVA and $S_{DGB,1}=S_{DGB,2}=S_{DGB,3}$=-1.80 MVA are satisfied. Since $|S_{LB,1}+\lambda_{LB,2}S_{LB,2}+S_{LB,3}+S_{LB,4}+S_{DGB,1}+S_{DGB,2}+S_{DGB,3}|\leq$1.60 MVA, the load power $\lambda_{LB,2}S_{LB,2}$ participating in DR increases from 0.00 to 1.80 MVA. According to the DG growth criticality equality constraint $\lambda_{LB,2}S_{LB,2}+S_{LB,3}+S_{LB,4}+S_{DGB,1}+S_{DGB,2}+S_{DGB,3}$=-1.60 MVA, it follows that $|\sum_{x=1}^{3} S_{DGB,x}|$=|-1.60-($\lambda_{LB,2}S_{LB,2}+S_{LB,3}+S_{LB,4}$)|=|-3.60-$\lambda_{LB,2}$|. Consequently, the TAC=$|\sum_{x=1}^{3} S_{DGB,x}|$ increases gradually from 3.60 to 5.40 MVA as $\lambda_{LB,2}$ increases, reaching a maximum value of 5.40 MVA.

In summary, DR participation improves the TAC only when the participating loads are located downstream of the bottleneck branch. Moreover, the magnitude of the improvement depends on the load location, and the TAC eventually reaches a plateau as the load adjustment coefficient increases.

5.3. Measures for Enhancing the TAC Curve

Based on the analysis in Section 5.2, two measures are proposed to improve the TAC curve:

Measure 1: Appropriately increase the load adjustment coefficients of loads participating in DR downstream of the bottleneck branch. The TAC curve is determined only by the loads downstream of the bottleneck branch, and its maximum value initially increases and then remains constant as the load adjustment coefficient increases.

Measure 2: Upgrade the capacity of the bottleneck branch. The capacity of the bottleneck branch is one of the primary factors limiting the TAC curve.

For example, the two aforementioned measures are implemented in the test system described in Section 5.1. Measure 1: The downstream load $S_{LB,2}$ participates in DR, with its load adjustment coefficient set to $\lambda_{LB,2}$=1.80. Measure 2: The capacity of bottleneck branch B_2 is increased from 1.60 MVA to 2.40 MVA. The improvements in the TAC curve achieved by these two measures are illustrated in Figure 8.

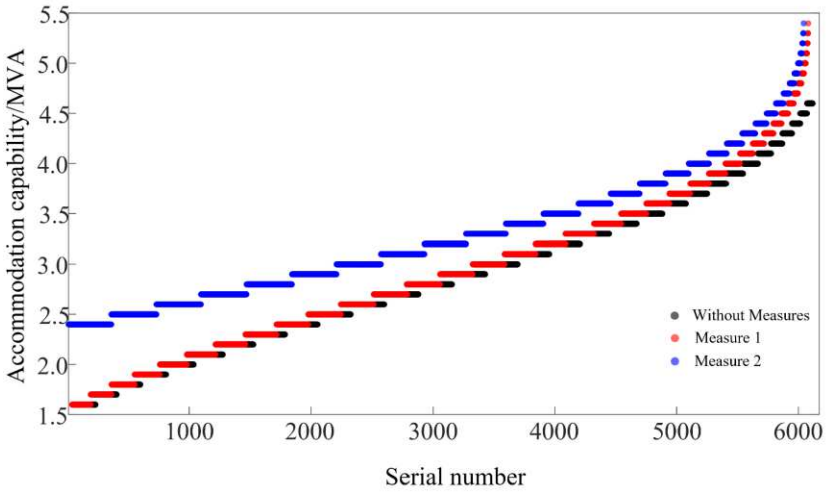

Figure 8. Effectiveness of TAC curve improvement measures.

As shown in Figure 8, both proposed measures can effectively enhance the TAC curve. After implementing Measure 1, the peak of the red TAC curve increases, with its maximum value rising from 4.60 to 5.40 MVA. Accordingly, the maximum TAC increases by 0.80 MVA, and the average TAC ($\overline{\text{TAC}}$) increases by 0.04 MVA. After implementing Measure 2, the peak of the blue TAC curve also increases, with its maximum value rising from 4.60 to 5.40 MVA. The maximum TAC increases by 0.80 MVA, the minimum TAC ($\text{TAC}_{\min}$) increases by 0.80 MVA, and the average TAC ($\overline{\text{TAC}}$) increases by 0.40 MVA.

The advantages and applicable scenarios of the two proposed enhancement measures are summarized as follows:

Measure 1: By appropriately increasing the load adjustment coefficients of loads participating in DR downstream of the bottleneck branch, the TAC curve can be enhanced to the greatest extent. This measure is applicable to scenarios in which the load side of a distribution network participates in DR.

Measure 2: By selectively upgrading the capacity of bottleneck branches, the TAC curve can be enhanced while effectively reducing the investment required for additional line capacity expansion. This measure is applicable to conductor replacement scenarios in bottleneck reinforcement projects of distribution networks.

5.4. Application of the TAC Curve to DR Decision-Making

As discussed in Section 5.2, both the degree of flexible load participation in DR and the locations of flexible loads affect the TAC curve. Therefore, the TAC curve can be used to guide users in making DR participation decisions.

（1）Selection of the DR load adjustment coefficient. The TAC curve reflects variations in the DG accommodation capability of distribution networks under different load adjustment coefficients. According to Figure 6 in Section 5.2.1, when the load adjustment coefficient $\lambda_{\text{LB},4}$ decreases from 1.00 to 0, the TAC decreases from 4.60 to 3.60 MVA. According to Figure 5 in Section 5.2.1, when the load adjustment coefficient $\lambda_{\text{LB},4}$ increases from 1.00 to 2.00, the TAC increases from 4.60 MVA to a maximum of 5.20 MVA. However, further increasing $\lambda_{\text{LB},4}$ does not lead to any additional increase in the TAC. Therefore, to enhance the TAC curve, the optimal value of $\lambda_{\text{LB},4}$ is 1.60. Further increases would only increase the load adjustment cost without yielding any additional improvement in the TAC.

（2）Selection of DR participation nodes. The TAC curve can be used to compare the improvements in DG accommodation capability achieved by flexible loads participating in DR at different locations. For example, according to Figure 7 in Section 5.2.2, DR participation by the upstream load $S_{\text{LB},1}$ of the bottleneck branch has no impact on the TAC. When the downstream loads $S_{\text{LB},3}$ and $S_{\text{LB},4}$ participate in DR, the maximum TAC reaches 5.20 MVA, whereas DR participation by the downstream load $S_{\text{LB},2}$ increases the maximum TAC to 5.40 MVA. Therefore, to enhance the TAC curve, priority should be given to loads located downstream of the bottleneck branch for DR participation, with the node corresponding to $S_{\text{LB},2}$ being the optimal location for user participation in DR.

6. Conclusions

To address the lack of a comprehensive characterization of the DG accommodation capability of distribution networks with flexible loads participating in DR in existing studies, this paper proposes a TAC curve for ADNs considering

DR. The main conclusions are summarized as follows:

（1）The proposed TAC curve model, which considers DR and voltage constraints, can comprehensively characterize the DG accommodation capability of ADNs with flexible loads participating in DR. The proposed TAC curve calculation algorithm, which accounts for flexible load adjustment characteristics, enables the determination of TAC curve indices under different DR participation locations and levels in distribution networks.

（2）The impacts of DR participation level and location on the TAC curve are revealed: DR participation enhances the TAC curve only when the participating loads are located downstream of the bottleneck branch, and the extent of TAC improvement varies depending on the locations of the participating loads. As the load adjustment coefficient increases, the TAC initially increases and then remains constant.

（3）The proposed measures of increasing the load adjustment coefficients of loads participating in DR downstream of the bottleneck branch and upgrading the capacity of the bottleneck branch can effectively enhance the overall DG accommodation capability of distribution networks.

（4）The TAC curve has significant practical value for DR decision-making in distribution networks and can provide guidance for users' DR participation decisions.

The proposed TAC curve for ADNs considering DR can effectively characterize the overall DG accommodation capability of distribution networks with flexible loads participating in DR, thereby providing a theoretical basis for exploiting the system's DG accommodation potential. Future work will further consider N-1 security constraints and energy storage systems, investigate the application of TAC curves in electricity markets, and analyze the impacts of different pricing and incentive mechanisms on load response behavior and DG accommodation capability.

Author Contributions: H.Y. conceived the conceptualization and methodology, acquired funding, and wrote the original draft. B.L. conducted the formal analysis and investigation. Y.W. developed the software and curated the data. W.C. performed the investigation and validation. W.X. handled the visualization and formal analysis. T.Y. provided the resources and contributed to writing—review and editing. X.Z. performed the validation and data curation. G.W. provided supervision and project administration. Z.Y. provided supervision. All authors discussed the results and approved the final manuscript.

Funding: This research was funded by the Science and Technology Project of State Grid Gansu Electric Power Company (Grant No. SGGSJC00FCJS2600520).

Data Availability Statement: The datasets used and analysed during the current study available from the corresponding author on reasonable request.

Conflicts of Interest: The authors declare no competing interests.

References

1. Fettah, K. et al. A pareto strategy based on multi-objective optimal integration of distributed generation and compensation devices regarding weather and load fluctuations. *Sci. Rep.* **14**, 10423 (2024).
2. Alromithy, F. S., Hosseinnia, H., Rostami, R. & Altimania, M. R. M. Investigating distributed generator high penetration in improving technical, emission and economic constraints of distribution network. *Sci. Rep.* **16**, 11430 (2026).
3. Loji, K., Sharma, S., Sharma, G. & Rawat, T. Multiobjective distribution system operation with demand response to optimize solar hosting capacity, voltage deviation index and network loss. *Sci. Rep.* **15**, 300 (2025).
4. Wang, C., Liu, C., Chen, J. & Zhang, G. Cooperative planning of renewable energy generation and multi-timescale flexible resources in active distribution networks. *Appl. Energy* **356**, 122429 (2024).
5. Varathan, G. & Belwin Edward, J. A review of uncertainty management approaches for active distribution system planning. *Renew. Sustain. Energy Rev.* **205**, 114808 (2024).
6. Qi, L., Li, Z., Wang, K., Liang, X. & Wang, C. Learning operational compatibility in distribution networks under multi-step renewable dynamics. *Sci. Rep.* **16**, 32629 (2026).
7. Jain, A. K. et al. Dynamic hosting capacity analysis for distributed photovoltaic resources—framework and case study. *Appl. Energy* **280**, 115633 (2020).
8. Cho, Y., Lee, E., Baek, K. & Kim, J. Stochastic optimization-based hosting capacity estimation with volatile net load deviation in distribution grids. *Appl. Energy* **341**, 121075 (2023).
9. Mulenga, E., Bollen, M. H. J. & Etherden, N. A review of hosting capacity quantification methods for photovoltaics in low-voltage distribution grids. Int. J. *Electr. Power Energy Syst.* **115**, 105445 (2020).
10. Tan, H. et al. A wind power accommodation capability assessment method for multi-energy microgrids. IEEE Trans. Sustain. *Energy* **12**, 2482–2492 (2021).
11. Liu, Y. et al. Evaluating smart grid renewable energy accommodation capability with uncertain generation using deep reinforcement learning. *Future Gener. Comput. Syst.* **110**, 647–657 (2020).
12. Zhu, X., Chen, L., Wang, T., Li, J. & Li, C. A bi-level optimization strategy for PV capacity configuration in active distribution networks considering time-series operation. *Sol. Energy* **312**, 114567 (2026).
13. Xiong, H., Zhou, Y., Guo, C., Ding, Y. & Luo, F. Multi-stage risk-based assessment for wind energy accommodation capability: a robust and non-anticipative method. *Appl. Energy* **350**, 121726 (2023).
14. Ye, L. et al. Study of assessment on capability of wind power accommodation in regional power grids. *Renew. Energy* **133**, 647–662 (2019).
15. Wang, Z., Jia, Y., Han, X., Wang, P. & Liu, J. Deep learning-based distributionally robust joint chance constrained distribution networks PV hosting capacity assessment. *Appl. Energy* **394**, 126130 (2025).
16. Pan, C., Chen, W., Zhou, C., Zhou, W. & Li, G. Research on enhancing RDGs accommodation and prolonging cable life via a combination of DTR, network reconfiguration and active controls. *Electr. Power Syst. Res.* **239**, 111223 (2025).
17. Xiao, J. et al. Total supply and accommodation capability curves for active distribution networks: concept and model. Int. J. *Electr. Power Energy Syst.* **133**, 107279 (2021).
18. Xiao, J. et al. The total accommodation capability curve for a distribution network considering N-1 criterion. Electr. *Power Syst. Res.* **243**, 111508 (2025).
19. Vallés, M., Bello, A., Reneses, J. & Frías, P. Probabilistic characterization of electricity consumer responsiveness to economic incentives. *Appl. Energy* **216**, 296–310 (2018).
20. Fan, W. et al. Distributionally robust optimization scheduling model for electric power and computing power coordination considering spatiotemporal response. *Appl. Energy* **402**, 126895 (2025).
21. Ding, B. et al. Optimization of unit commitment considering multiple stochastic factors and interruptible load under chance constraints. *Sci. Rep.* **16**, 1788 (2026).
22. Zeng, B., Zhao, D., Singh, C., Wang, J. & Chen, C. Holistic modeling framework of demand response considering multi-timescale uncertainties for capacity value estimation. *Appl. Energy* **247**, 692–702 (2019).
23. Zu, G., Xiao, J. & Sun, K. Mathematical base and deduction of security region for distribution systems with DER. *IEEE Trans. Smart Grid* **10**, 2892–2903 (2019).
24. Qu, Y., Xiao, J. & Zu, G. Security region and power supply capability for distribution system under normal operational state: definition, model, and application. *CSEE J. Power Energy Syst.* **12**, 1896–1913 (2026).
25. Xu, X., Jia, Y., Lai, C. S., Wang, M. & Xu, Z. Bi-level optimal planning of voltage regulator in distribution systems considering maximization of incentive-based photovoltaic energy integration. *CSEE J. Power Energy Syst.* **9**, 2008–2017 (2023).
26. Qi, Z., Guo, S. & Zhao, H. Research on quantitative evaluation and optimal allocation of electricity system flexibility. *Energy* **320**, 135443 (2025).

27. Li, S. et al. Two-stage voltage control strategy in distribution networks with coordinated multimode operation of PV inverters. *IET Renew. Power Gener.* **17**, 66–82 (2023).